Journal Name

ARTICLE

Ferrocenylethenyl-substituted oxadiazoles with phenolic and nitro anchors as sensitizers in dye sensitized solar cells

Received 00th January 20xx,
Accepted 00th January 20xx

DOI: 10.1039/x0xx00000x

www.rsc.org/

Amita Singh, [a] Gabriele Kociok-Köhn,[b] Manoj Trivedi,[c] Ratna Chauhan,[d]* Abhinav Kumar,[a]* Suresh S. Gosavi[e], Chiaki Terashima[f] and Akira Fujishima[f]

Three new ferrocenyl oxadiazoles *viz.* (*E*)-2-(4-hydroxyphenyl)-5-(2-ferrocenyl-ethen-1-yl)-1,3,4-oxadiazole (**D2**), (*E*)-2-(4-nitrophenyl)-5-(2-ferrocenyl-ethen-1-yl)-1,3,4-oxadiazole (**D3**) and (*E*)-3-(4-nitrophenyl)-5-[5-(2-ferroceneylethen-1-yl)-1,3,4-oxadiazol-2-yl]-1,2,4-oxadiazole (**D4**) derived from (*E*)-3-ferrocenylacrylic acid (**D1**) having phenolic or nitro anchors have been synthesized and characterized using microanalyses and relevant spectroscopic techniques. UV-Vis spectroscopic studies indicate that with respect to ferrocene the electronic absorption bands new compounds are bathochromically shifted up to 600 nm with concomitant enhancement in their intensities. All four compounds have been used as photosensitizers in TiO_2-based dye-sensitized solar cells (DSSCs). The photovoltaic performances and charge transport properties (EIS spectra) of these compounds were studied to appraise their dye performance. All four compounds displayed good photovoltaic performances. However, compounds **D2** and **D4** displayed superior performance which might be due to the better electronic communication between the ferrocenyl moiety and the six membered aromatic ring with their –OH/NO_2 anchors through five membered oxadiazole spacers, as well as the high dye loading of these compounds on the TiO_2 surface, which suppresses charge recombination, prolongs electron lifetime, and decreases the total resistance of DSSCs. The assembly fabricated using **D4** performed superior with an overall conversion efficiency η of 4.70%, J_{sc} of 10.33 mA.cm^{-2} and V_{oc} of -0.712 V.

Introduction

During the past two decades dye-sensitized solar cells (DSSCs), have been attracting enormous attention amongst the scientific community[1, 2] as they offer edge over the conventional photovoltaic devices such as they are light weight, colored and flexible and have established power conversion efficiency reported from 11.4%[3] to 14.3%.[4] The key component in DSSCs are sensitizers which play crucial role in DSSCs as they control the light harvesting and charge separation properties.[1] Additionally, the structure of sensitizers can be modified to enhance the molar extinction coefficient as well as the solar light harvesting capacity. This objective can be accomplished by modifications in the chromophore and anchoring group which therefore can improve the photocurrent and efficiency of DSSC.[5-7] Several metal based sensitizer *viz.* Ru-based dyes,[8] Zn porphyrins and pervoskites[9] have shown remarkable power conversion efficiency (PCE). However, their high cost especially the Ru-based dyes limit their practical implementation.

To resolve this issue, several organic dyes possessing versatile structures have been employed as sensitizers in DSSCs. Organic dyes comprising of triphenylamine (TPA) donors and different π-conjugated linkers such as aromatic and heteroaromatic moieties with cyanoacrylic acid as anchoring/acceptor group were best suited to enhance the photovoltaic performances of DSSCs.[10]

During recent years we have been continuously working to develop ferrocene and its derivatives as possible photo-sensitizers that can be used in DSSC. In our pursuit to develop potential ferrocene based sensitizers we have reported the light harvesting properties of the homo- and heteroleptic complexes of ferrocenyl dithiocarbamates,[11-14] and their organomercury(II) derivatives.[15,16] We also worked on ferrocene dithiocarbamate and dithiocarbonate as anchors in DSSCs.[17] In addition to these sulphur derivatives π-conjugated derivatives of ferrocene and biferrocene with different anchors have been reported by our group.[18-21] Recently, we deployed 1,1'-bis(diphenylphosphino)ferrocene appended Ni(II) ditihiolates as sensitizers[22] but they displayed modest photovoltaic efficiencies due to an unfavourable charge transfer direction.[22] Mishra *et. al* reported ferrocenyl substituted triphenylamine based donor–acceptor dyes for dye sensitized solar cells.[23] Sirbu *et al*. found that DSSCs fabricated using a trisubstituted ferrocene-based porphyrin derivative with a Co^{2+}/Co^{3+} electrolyte, resulted in

[a] *Department of Chemistry, Faculty of Science, University of Lucknow, Lucknow 226007, India, Email: abhinavmarshal@gmail.com*
[b] *Materials and Chemical Characterisation Facility (MC²), University of Bath, Bath, BA2 7AY, UK.*
[c] *Department of Chemistry, University of Delhi, Delhi, India*
[d] *Centre for Materials for Electronics Technology, Pune, India Email: ratnasingh.bhu@gmail.com*
[e] *Department of Physics, University of Pune, Pune*
[f] *Photocatalysis International Research Center, Research Institute for Science & Technology, Tokyo University of Science, 2641 Yamazaki, Noda, Chiba 278-8510, Japan*

Electronic Supplementary Information (ESI) available: [details of any supplementary information available should be included here]. See DOI: 10.1039/x0xx00000x

only modest conversion efficiency[24]. Cariello and co-workers designed some ferrocenyl based dyes and investigated the role of π-conjugation on the conversion efficiency.[25] The choice of using ferrocene derivatives as sensitizers is down to the well-defined reversible one-electron redox process[26-28] and electron donating properties.[26,29,30] The formal reduction potential of the ferrocenyl group depends on the nature of the substituents on the cyclopentadienyl ring. The redox potential can be tuned to obtain the desired potential for a specific application.[26,30,31]

In continuation to our development program for photosensitizers comprising of ferrocene, we found that oxadiazole derivatives which exist in four regioisomeric forms (two 1,2,4-isomers, if asymmetrically substituted, a 1,3,4-isomer, and a 1,2,5-isomer) have been used as luminescent materials[32] as well as sensitizers in DSSCs.[33] Their electron withdrawing effects have been utilized to develop charge-transfer species.[34] In addition to common oxadiazoles connected with aromatic rings, the ferrocenyl derivatives of oxadiazoles have been reported.[35] These ferrocenyl oxadiazoles have been investigated for DNA binding assay[35a] and antimicrobial activity.[35c] Although, the biological properties associated with ferrocenyl based oxadiazoles are reported but to the best of our knowledge the applications of ferrocenyl oxadiazoles as sensitizers in DSSCs have not been reported. In the expedition of new ferrocene based sensitizers we have synthesized three new ferrocenylethynyl-substituted oxadiazoles and tested their ability as sensitizers in DSSCs. The results of these investigations are presented herewith.

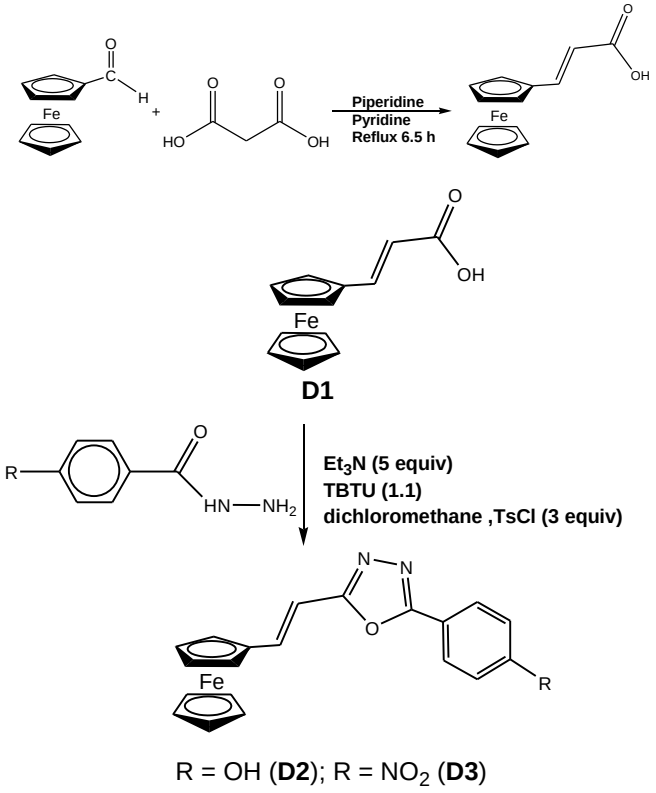

Scheme 1. Synthetic routes for the sensitizers **D1**, **D2** and **D3**.

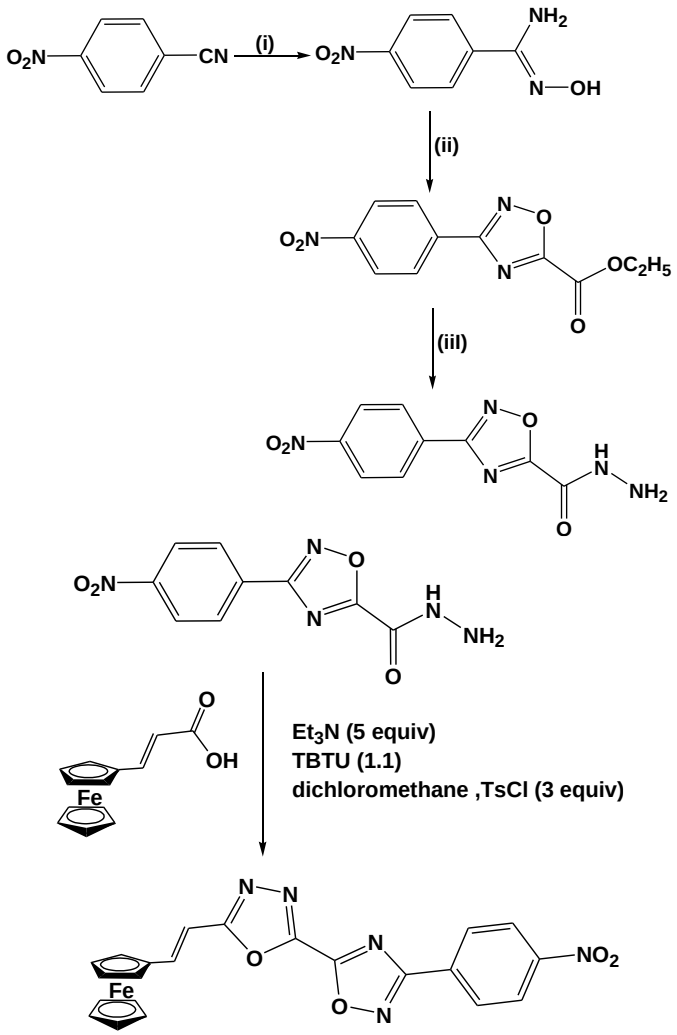

Scheme 2. Synthetic routes for the sensitizer **D4**

Conditions: i) $NH_2OH.HCl$, NaOH; EtOH, H_2O, r.t. 15h. ii) Et_2O_2CCOCl, DIPEA; THF, reflux, 2h. iii) $NH_2NH_2{\cdot}H_2O$; EtOH, r.t.; 1h.

Results and discussion

The ferrocenecarboxaldehyde was condensed with malonic acid in refluxing pyridine/piperidine following the Knoevenagel-Doebner reaction procedure to produce (*E*)-3-ferrecenylacrylic acid (**D1**) in moderate yield (Scheme 1). The condensation of (*E*)-3-ferrecenylacrylic acid with aromatic acid hydrazides yielded the desired ferrocenyl 1,3,4-oxadiaoles *viz.* (*E*)-2-(4-hydroxyphenyl)-5-(2-ferrocenyl-ethen-1-yl)-1,3,4-oxadiazole (**D2**) and (*E*)-2-(4-nitrophenyl)-5-(2-ferrocenyl-ethen-1-yl)-1,3,4-oxadiazole (**D3**) (Scheme 1). In order to obtain (*E*)-3-(4-nitrophenyl)-5-[5-(2-ferroceneylethen-1-yl)-1,3,4-oxadiazol-2-yl]-1,2,4-oxadiazole (**D4**), the hydrazide was prepared using a three step process, starting with the synthesis of amidoxime by treating 4-nitro benzene nitrile with hydroxylamine hydrochloride and aqueous sodium hydroxide ethanol at room temperature for 15 h. Thereafter amidoxime was condensed with ethyl oxalyl chloride, employing DIPEA as base, in tetrahydrofuran at 0 ºC and the reaction mixture was refluxed for ~2 h, giving the corresponding 1,2,4-oxadiazole. Hydrazinolysis

of the ester in ethanol by action of aqueous hydrazine at room temperature for 1 h yielded 3-(4-nitrophenyl)-1,2,4-oxadiazole-5-carbohydrazide. The obtained final product was condensed with (*E*)-3-ferrecenylacrylic acid similar to **2** and **3** to get (*E*)-3-(4-nitrophenyl)-5-[5-(2-ferroceneylethen-1-yl)-1,3,4-oxadiazol-2-yl]-1,2,4-oxadiazole (**4**) (Scheme 2).

Spectroscopy and X-ray structure description

The sensitizers were characterized using FTIR, ^{1}H and ^{13}C NMR spectroscopy as well as high resolution mass spectrometry. The purity and composition of all sensitizers were assessed with ^{1}H NMR spectroscopy which display well resolved signals that integrated well to the corresponding hydrogens (*vide infra*). In the ^{13}C NMR spectra for the dyes **D2**-**D4** the resonances lying in the region ~δ 140-165 ppm correspond to oxadiazole ring. The IR spectra of the four dyes show the bands arising at ~3070 cm^{-1} can which be assigned to the ν_{C-H}. The dye **D1** displays a band near 1668 cm^{-1} which corresponds to ν_{COOH}. In **D2** the band at 3490 cm^{-1} can be ascribed to ν_{OH}. The bands arising at 1610 (**D1**), 1604 (**D2**), 1631 (**D3**) and 1641 cm^{-1} (**D4**) are because of $\nu_{C=C}$. In **D3** and **D4**, bands at 1519 and 1523 cm^{-1} corresponds to the $\nu(NO_2)$asymm for **D3** and **D4**, respectively, while bands appearing at 1338 and 1350 cm^{-1} can be attributed to $\nu(NO_2)$symm for **D3** and **D4**, respectively. Also, in all the dyes bands at ~1450-1490 cm^{-1} and ~1260 cm^{-1} correspond to the presence of oxadiazole ring. Additionally band at ~490 cm^{-1} may be arising because of the stretching vibration from the Fe-Cp ring.

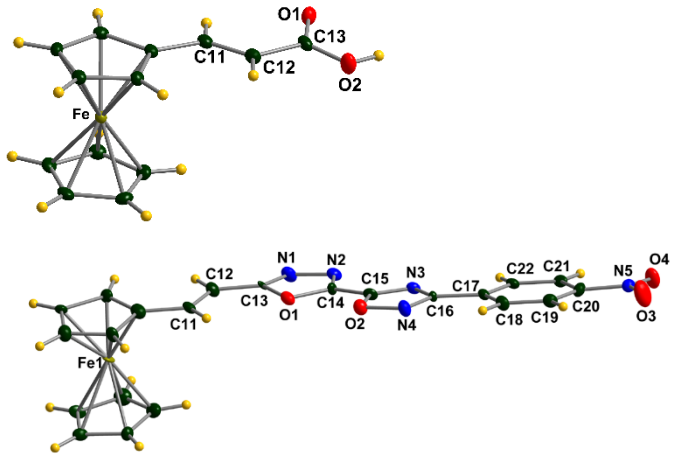

Fig. 1 Perspective views of the sensitizers **D1** (above) and **D4** (below).

The perspective view of the dyes **D1** and **D4** are presented in Fig. 1. The X-ray structures for both the sensitizers indicate that the exo-cyclic double bond lying in vicinity to ferrocenyl moiety acquires *E* configuration. In the case of **D1** the dihedral angle between the plane formed by five membered Cp ring and olefinic carbon center is 3.38º. In the case of **D4** the two oxadiazole ring are exactly planar while the dihedral angle between the 1,2,4-oxadiazole ring and the six membered ring is 1.93º. The dihedral angle between the Cp ring and 1,3,4-oxadizaole unit is 6.13º. This indicates that the **D4** is highly planar molecule and can offer excellent electronic communication between ferrocenyl and nitro-aromatic entity. Further the composition of these sensitizers had been confirmed with the aid of HRMS experiments (*vide infra*).

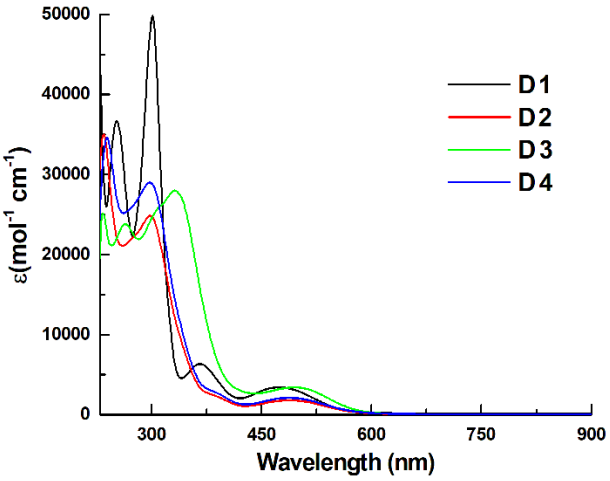

Fig. 2 Electronic absorption spectra for sensitizers recorded in 10^{-4} M dichloromethane solution.

The electronic absorption spectra for the sensitizers were recorded in dichloromethane solution (Fig. 2) which display absorption maxima in the visible region ranging between 470 to 500 nm. This band is arising due to the d →d transition (assigned to $^{1}E_{1g} \leftarrow {}^{1}A_{1g}$).[36] In comparison to **D1** which is the base unit of the sensitizers the band is red shifted in dyes **D2**, **D3** and **D4**. The bathochromic shifting may be accredited to extensive conjugation between the ferrocenyl moiety to the six membered aromatic ring with anchoring groups *via* the olefinic moiety and the oxadiazole linkage. This leads to a strong electronic communication between ferrocene to the aromatic fragment to which the anchors are attached. This spectral feature prompted us to deploy these molecules as potential sensitizers in DSSC.

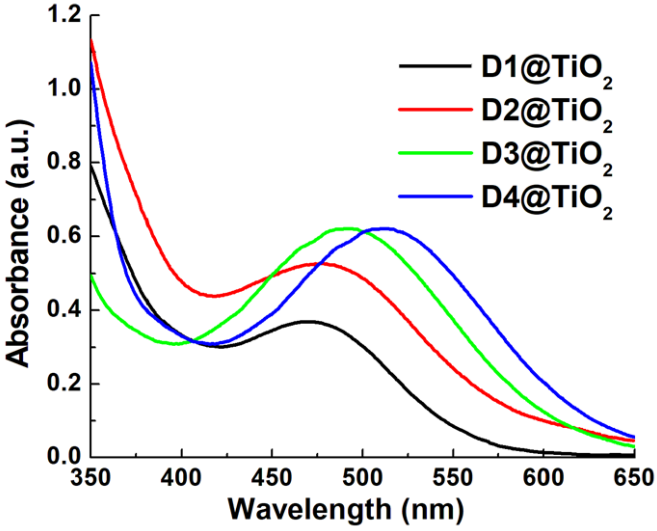

Fig. 3 Electronic absorption spectra of dyes adsorbed at TiO_2 nanoparticulate.

The electronic absorption spectra of the dyes recorded on a TiO_2 film (Fig. 3) shows slight broadening in the maxima range with minor bathochromic shifts which may arise because of aggregation of the dyes[37] or electronic coupling of the dyes on the TiO_2 surface.[38]

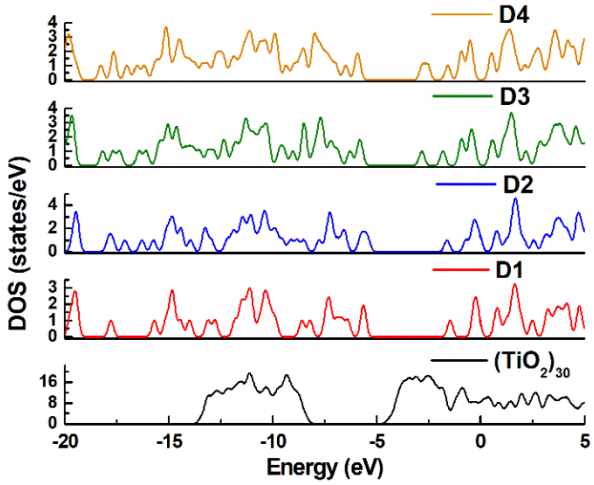

Fig. 4 Density of states plots for $(TiO_2)_{30}$ nanocluster and dyes **D1** to **D4**.

Electron injection

To assess whether electrons can be injected by dyes **D1**-**D4** in the conduction band of TiO_2 nanoparticulte, we have performed density of states (DOS) calculations on $(TiO_2)_{30}$, dyes **D1**-**D4** as well as dye+$(TiO_2)_{30}$ systems. The results of these calculations are presented in Figs. 4 and 5. Figure 4 reveals that in comparison to the DOS of $(TiO_2)_{30}$ cluster, the DOS of the dyes shows clearly localized states, which are all occupied (Fig. 4). In the case of dye+$(TiO_2)_{30}$, the DOS plot clearly indicates core states, valence band (VB), and conduction band (CB). The fundamental valence band in $(TiO_2)_{30}$ is located at the energy levels roughly between –10.0 eV and –8.2 eV, and the conduction band is located starting from –4.6 eV. The DOS plot for the $(TiO_2)_{30}$ cluster displayed a clear separation between VB and CB without any gap states (Fig. 4). The adsorption of the dyes onto the nanoparticle surface introduces occupied states at the lower part of the nanoparticle band gap and extending the valence states from around –8.2 eV to –5.6, –5.3, –5.5 and -5.5 eV for **D1**@$(TiO_2)_{30}$, **D2**@$(TiO_2)_{30}$, **D3**@$(TiO_2)_{30}$ and **D4**@$(TiO_2)_{30}$, respectively (Fig. 5). Based on the DOS plots (Fig. 5), it can be inferred that lower energy electrons are excited from VB energy levels approximately between –8.2 and –5.6 to –5.3 eV for dye@$(TiO_2)_{30}$ and then transferred to CB states above –4.6 eV. Based on the DOS plot, the minimum inter-band excitation energy lie in the range of 0.7-1.0 eV for dye@$(TiO_2)_{30}$ systems. The results of DOS indicates significant electronic coupling between the LUMO of dyes and the CB of TiO_2, which facilitates the electron injection from photo-excited dyes in the conduction band of TiO_2 nanoparticle.

Electrochemical properties

Further evaluation of thermodynamic feasibility of dye regeneration and electron transfer process from photo-excited dye to conduction band of TiO_2 the position of HOMO and LUMO energy levels have been estimated electrochemically using cyclic voltammetry (Fig 6). From cyclic voltammetry it was inferred that the dyes **D1** to **D4** were highly active towards photoredox processes. Cyclic voltammetry experiments were carried out in a three-electrode cell on an electrochemical workstation using a Pt disc as working electrode and Ag/Ag+ (in acetonitrile) as reference electrode in dichloromethane containing 0.1 M tetra-n-butylammonium perchlorate. The electrochemical parameters for the dyes are summarized in Table 1.

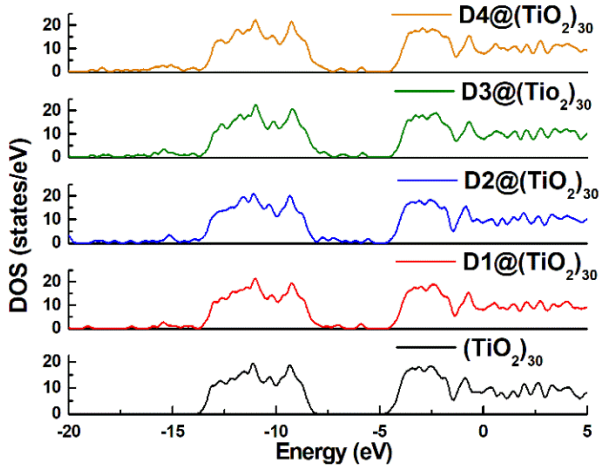

Fig. 5 Density of states plots for $(TiO_2)_{30}$ nanocluster and dyes@$(TiO_2)_{30}$.

Table 1. Electrochemical parameters of the dyes (D-1 to D-4) calculated from cyclic voltammogram

Dyes	$E_{p,a}$ (V)	$E_{p,c}$ (V)	Δ E = $E_{p,a}$- $E_{p,c}$ (V)	E^o (V) = ($E_{p,a}$+ $E_{p,c}$)/2	$E.S$= E^o + hv
D-1	+0.650	+0.440	+0.210	+0.545	-1.96
D-2	+0.704	+0.464	+0.240	+0.584	-1.98
D-3	+0.686	+0.252	+0.435	+0.469	-2.06
D-4	+0.568	+0.352	+0.216	+0.460	-2.16

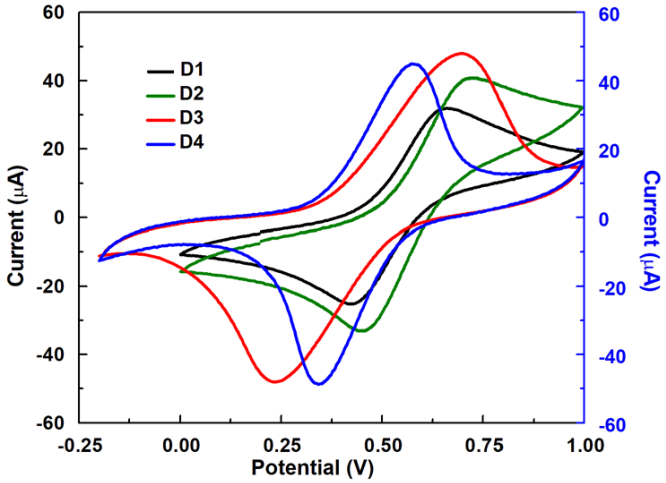

Fig 6 Cyclic voltammogram for the dyes recorded in 10^{-3} M dichloromethane solution

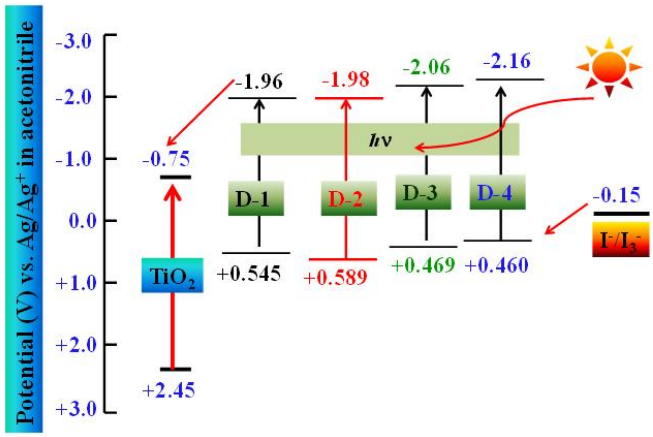

Fig. 7 Energy level diagram for the cell assembly fabricated by sensitizers D1 to D4.

From Table 1 it is apparent that the excited-state of the dyes are sufficiently negative (–2.16 to –1.96 V vs. Ag/Ag+ in ACN) than the conduction band edge of TiO_2 (–0.75 V vs. Ag/Ag+ in ACN), which ensures an energetically favourable electron injection from the photo-excited dye to TiO_2 and that the ground states of the dyes are more positive (+0.545 to +0.460 V vs. Ag/Ag+ in acetonitrile) which suggests a thermodynamically sufficient driving force for the regeneration of the dyes (Fig. 7). Furthermore, the energy level diagram (Fig 7) for the four dyes shows favourable excited-state oxidation potential with respect to the TiO_2 conduction band. This would ensure better electron transfer, electron collection which results in higher photocurrent, and better cell efficiency while favourable ground-state reduction potential ensures the dye regeneration capability.

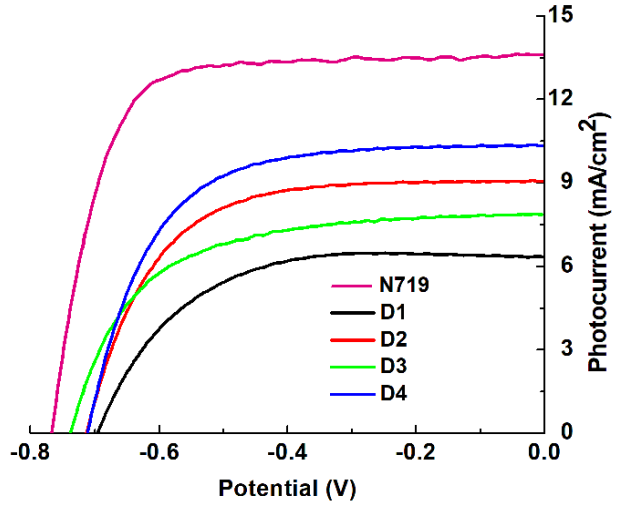

Fig. 8 *J–V* curves for DSSCs based on dyes D1 to D4 sensitized photoelectrodes

Photovoltaic measurements

To study the photovoltaic properties of the DSSCs fabricated with the **D1** to **D4** dyes, the J-V curves were recorded (Fig. 8). The DSSCs Parameters such as V_{oc}, short-circuit current density (J_{sc}), fill factor (FF), η and the maximum values of IPCE are summarized in 2. The highest cell efficiency η (4.7%) was found in the case of the **D4** dye, although the incorporation of two oxadiazole units serving as π-bridging group in **D4** caused a slight decrease in the V_{OC} (0.712V) than **D3** comprising of only one oxadiazole unit V_{OC} (0.736V). The J_{SC} was observed to increase significantly from 7.85 to 10.33 mA·cm^{-2} for **D3** to **D4** on incorporation of an additional oxadiazole unit leading to higher efficiency in **D4** probably resulting from better electron separation. The dye **D2** shows the second highest efficiency among all dyes due to the –OH group which offers better anchorage on the TiO_2 surface thereby leading to a maximum photon absorption for current conversion (Table 2).

Table 2: Photovoltaic parameters for the dyes D-1 to D-4

Dyes	J_{sc} (mAcm^{-2})	V_{oc} (V)	*FF*	η(%)	*Max. IPCE* (%)	Dye Loading amount (mmol. cm^{-2})
N719	13.62	-0.77	0.73	7.70	55	3.78×10^{-7}
D-1	6.35	-0.696	0.61	2.71	51	2.79×10^{-7}
D-2	9.05	-0.711	0.64	4.11	55	2.94×10^{-7}
D-3	7.85	-0.736	0.61	3.52	53	2.81×10^{-7}
D-4	10.33-	-0.712	0.64	4.70	58	2.95×10^{-7}

Figure 9 presents the IPCE spectra of the DSSCs photosensitized by dyes **D1**-**D4** which are recorded in the region of 400–700 nm. The results of the IPCE measurements are consistent with the results of current-potential curves. The close resemblance were observed between the electronic absorption spectra of dyes with their respective IPCE spectra, except for a minor red shift by *ca.* 3–4 nm. This confirms the sensitization of the photocurrent by dye. The strong blue light absorption by I^-/I^{3-} redox couples present in electrolyte have been considered to decrease the IPCE value at shorter wavelength region,[39] resulting in the slight red shift in the bands in IPCE spectrum. The DSSC assembly with dye **D4** showed maximum IPCE value of 58% at 500 nm. The trend of IPCE maxima in decreasing order is **D4>D2>D3>D1**, which is in good agreement with photocurrent of respective dyes.

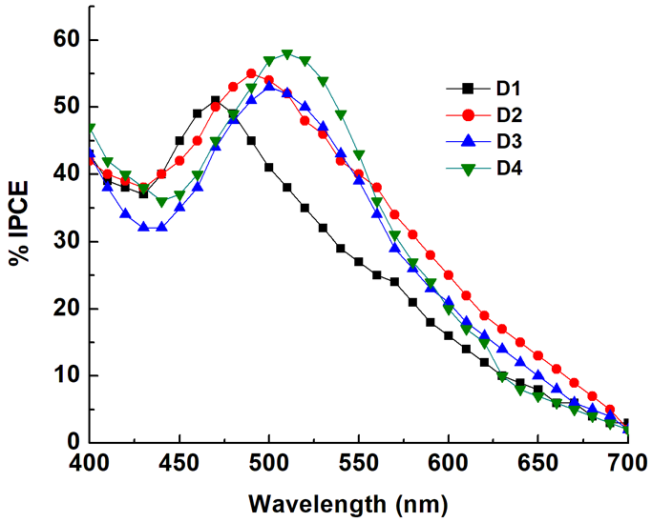

Fig. 9 IPCE plots for the dyes D1 to D4.

Previously in our quest for the synthesis of ferrocene based dyes to be used as sensitizers in DSSCs, we have synthesized ferrocenyl dithiolate complexes with no specific anchoring groups. These dyes acted as photosensitizers through remote sensing or physical adsorption on the TiO_2 surface and have spectral response in the range of 400-440 nm.[11, 12, 14, 15] Our recent investigation with phenylmercury(II) methylferrocenyldithiocarbamates with –OH linker[16] enhances the photovoltaic performance. To overcome the anchoring problem we designed π-extended ferrocenes with a variety of anchoring groups which provided better anchorage than the previous dyes and gave better results,[17-21] which enabled us to enhance the spectral response in the visible region beyond 450 nm. With the ferrocenyl oxadiazoles reported herein we succeeded in extending the spectral response into the visible region up to 600 nm. The presented results are encouraging and clearly indicates that the photovoltaic parameters of ferrocenyl oxadiazoles as photosensitizers are akin to the state-of-the-art **N719** dye and these ferrocenyl oxadiazole dyes with some fine tuning may become promising candidates for the realization DSSC assembly with good- cell performance.

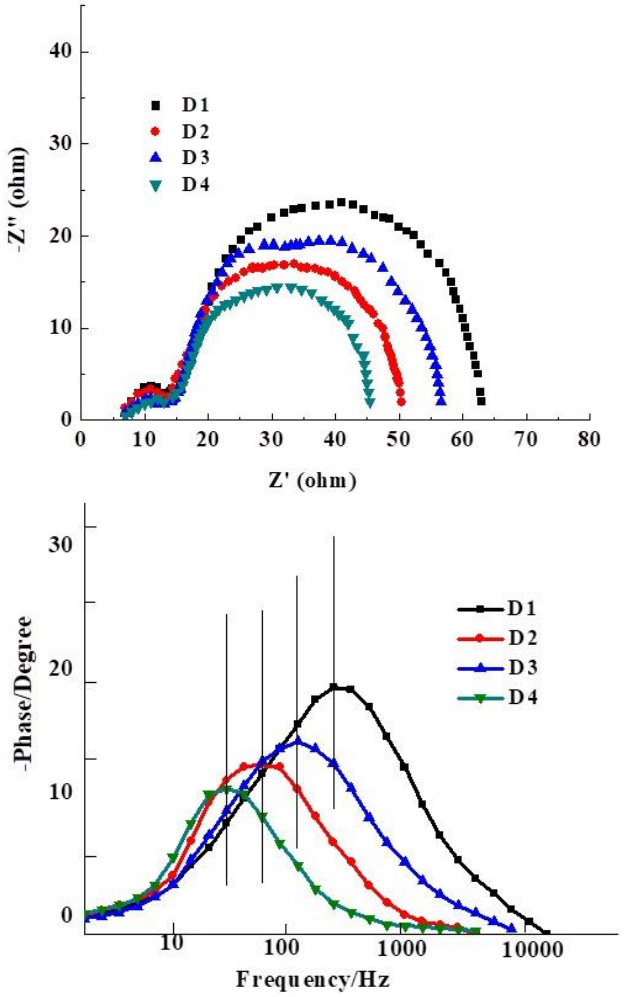

Fig. 10 Electrochemical impedance spectra of DSSCs measured at V_{oc}, 100 mWcm^{-2}: (a) Nyquist plots and (b) Bode plots.

EIS Measurements

Electrical impedance spectroscopy (EIS) is a useful analytical tool to investigate the electron transport properties at DSSC interfaces and its correlation with the performance at their open circuit potential (OCP) over a frequency range of 10^{-2}–10^5 Hz under 1.5 AM.

There are different processes that occur in the cell under illumination: The transfers of electrons from dyes to the conduction band of TiO_2, electrons are transported through the TiO_2 system and react with I^{3-}. At the same time I^- is oxidized to I^{3-} (dye regeneration) at the counter electrode. The Nyquist and Bode plots for the dye (**D1** to **D4**) sensitized cells are shown in Figure 10a and b, respectively. The presence of two semicircles in the Nyquist plots can be attributed to charge transfer reactions at interfaces as the appearance of the first smaller semicircle is ascribed to charge transfer at the Pt/electrolyte interface. The second larger semicircle in the middle frequency region stand for the charge transfer processes at the TiO_2/dye/electrolyte interface at the bias applied voltage. The semicircle diameter for TiO_2/dye/electrolyte interface decreases as the charge transfer resistance decreases upon illumination of cell.

The decrease in charge transport resistance in the middle frequency region is **D4>D2>D3>D1**, which follows the same trend as photocurrent results obtained from the ferrocene oxadiazole based DSSCs. The decreasing trend of recombination rates are **D1>D3>D2>D4**, which supports the higher V_{oc} values for **D2**, **D3** and **D4**. The Bode phase plots (Fig. 10b) have been obtained to determine the effective lifetime (t_{eff}) which explains further the higher V_{oc} values of dyes by electron lifetime. The value of the frequency for dyes **D1**, **D2**, **D3** and **D4** is 47.32, 32.65, 39.23 and 23.06 Hz, respectively, with effective life times of 3.36, 4.87, 4.05 and 6.90 ms, respectively. These results have been obtained using the following equation.[40]

$$t_{eff} = 1/2\pi f$$

where the frequency (f) corresponds to the maximum frequency of the mid-frequency peak in the Bode phase plot. The lowest electron lifetime in the case of **D1** in comparison to other dyes could explain the lowest V_{oc} value for **D1** sensitized cell. The highest performance of the **D4** based cell is due to the presence of two oxadiazole spacer as π-linker which provides better electronic communication to inject electrons efficiently in the conduction band of TiO_2 as well as the lowest electron transport resistance value, which acts as a driving force for the highest J_{sc} and V_{oc} for **D4**.

IMVS and IMPS study

Intensity modulation photovoltage spectroscopy (IMVS) and intensity modulation photocurrent spectroscopy (IMPS) studies in DSSCs are important tools to determine the electron lifetimes (τ_n) and electron transit times (τ_d).[41, 42] The parameters τ_n and τ_d are important as they imply recombination lifetime of electrons in the electrolyte and transport lifetime of the photo-generated electrons within the photoanode film. Figure 11 displays the results of IMVS and IMPS investigations for **D1** to **D4** based cell. The IMVS study indicates that the back reaction between the electrons in the TiO_2 conduction band and I^{3-} in the

electrolyte is mainly responsible for charge recombination in DSSCs thereby resulting in decline in electron lifetime as well as poor device performance. The IMVS and IMPS results shows the lower electron lifetime (τ_n) and higher transport time for **D1** based cell in comparison to rest of the three dyes with the oxadiazole spacers. These results are in agreement with the results of EIS measurements. This is probably happening due to the strong aggregation of **D1** dye on the TiO_2 surface owing to its large dipole moment. The dyes **D2**, **D3** and **D4** based cells show lower recombination than the **D1** based cell. The reason is that these dyes possess auxiliary acceptor unit (oxadiazole unit) into the D-π-A skeleton, which is responsible for improved electron lifetime in the devices. This leads to the enhanced charge separation and electron injection from the dyes to the conduction band of TiO_2. Amongst the three ferrocenyl oxadiazole based dyes, the **D4** based assembly shows highest photocurrent and cell efficiency as it contains two oxadiazole spacer units which result in efficient charge separation and lower recombination rate. Therefore the cell performance can be enhanced by introducing suitable linker and π acceptor group which facilitate the lowering of the energy barrier and recombination rate which thereby stimulate superior electron transport as well as high charge collection efficiency.[43]

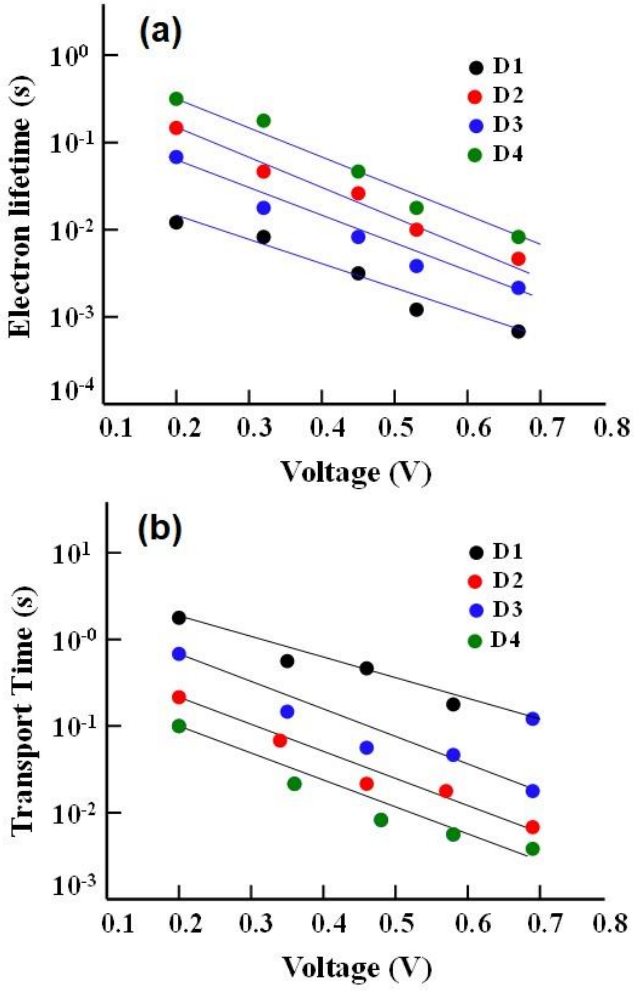

Fig. 11 The (a) electron life time and (b) transport time for dye D-1 to D-4 as photosensitizers with TiO_2 in DSSCs as a function of open-circuit voltage

Conclusions

The presented investigation shows that ferrocenyl oxadizole dyes with phenolic and nitro anchoring groups can be utilized as donor type sensitizers. By using these dyes, the spectral response of a wide band gap TiO_2 electrode can be extended well into the visible region (up to 600 nm wavelength). The photo-action spectra for the DSSCs fabricated using these compounds provide strong evidence for their sensitization effect on the TiO_2 photoanode. We have succeeded to achieve a maximum of ~61% of cell efficiency compared to the **N719** dye using these ferrocenyl oxadiazole dyes. Looking into the techno-economic aspects of these ferrocen oxadiazole based dyes could be a serious alternative for the **N719** dye. We have also shown that incorporation of an extra oxadiazole spacer between the six membered aromatic ring with anchoring group and the ferrocenyl moiety improved the electronic communication operating from the ferrocenyl fragment to the six membered aromatic ring, which in turn improved the photovoltaic parameters of the device. Broadening and enhancement in the spectral response into the visible region, down to a suitable anchoring group and electron communication properties associated with the ferrocenyl oxadiazole systems makes them an attractive candidate for enhancing the cell efficiency in DSSCs.

Experimental

Materials and Methods

All chemicals and reagents were commercially available and used without further purification. Ferrocene carboxaldehyde, malonic acid, TBTU, 4-hydroxybenzhydrazide, 4-nitrobenzhydrazide, 4-nitrobenzonitrile, N,N'-diisopropylethylamine, ethyl oxalyl chloride, hydrazine hydrate were purchased from Sigma-Aldrich while the remaining chemicals were from TCI chemicals.

Physical measurements. Elemental analyses were performed on a Perkin-Elmer 240 C, H, N analyzer. Infrared spectra were recorded as KBr pellets on a Shimadzu IRAffinity-1S. ^1H and ^{13}C NMR spectra were recorded on a BRUKER Avance III FTNMR spectrophotometer. Chemical shifts were reported in parts per million using TMS as internal standard. The electronic absorption spectra in dichloromethane solution were recorded using a SPECORD 210 PLUS BU UV-Vis spectrophotometer. Electrochemistry was carried out using a Pt working electrode, Pt rod counter electrode and Ag/AgCl as a working electrode. All electrochemical experiments were carried out in dichloromethane. In all cases TBAP (0.1 M) was used as supporting electrolyte. After each experiment the reference electrode was calibrated against the ferrocene/ferrocenium couple which was found to be at 0.55 V. The photoelectrochemical performance, including the short-circuit current (J_{sc}, mA/cm^2), open-circuit voltage (V_{oc}, V), fill factor (*FF*), and overall energy conversion efficiency (η) were determined from the *J–V* curve obtained by using a digital Keithley 236 mm under an irradiation of white light from a 1000 W/HS Xenon arc lamp with a 100 mW/cm^2 light intensity with 1.5 AM. The maximum output power (P_{max}) was obtained by

choosing a point on *J-V* curve corresponding to which the product of current (J_{max}) and voltage (V_{max}) is maximum. The power conversion efficiency (η) and fill factor (*FF*) were evaluated using the following relations:

$$FF = \frac{J_{\max}(\mathrm{A/cm^2}) \times V_{max}(\mathrm{V})}{J_{\mathrm{SC}}(\mathrm{A/cm^2}) \times V_{\mathrm{OC}}(\mathrm{V})}$$

$$\eta(\%) = \frac{J_{\mathrm{SC}} \times V_{\mathrm{OC}} \times FF}{I_{\mathrm{inc}}\,(\mathrm{W/cm^2})} \times 100$$

Here J_{sc}, V_{oc} and I_{inc} are short-circuit photocurrent, open-circuit potential and intensity of incident light respectively.

To avoid spurious light reflections and refractions a black mask was used for the cell on the illuminated side and also used to cover the side area of the cell, which largely contributed to the cell response and lead to erroneous interpretation. The reproducibility and reliability of the results was confirmed by creating three cells of each sensitized photoanode and keeping all structural and photovoltaic characterization identical. The active area of the cells was 0.25 cm^2.

The incident photon-to-electron conversion efficiency (*IPCE*) was measured by using a 300 W Xe lamp light source joined to a monochromator (Oriel). A reference Si photodiode calibrated for spectral response was used for the monochromatic power-density calibration. From the values of J_{sc} and the intensity of the corresponding monochromatic light (I_{inc}), the incident photon-to-current conversion efficiency (IPCE) was calculated at each excitation wavelength (λ) using the following relation:

$$IPCE\ (\%) = \frac{1240\ J_{\mathrm{sc}}(\mathrm{A/cm^2})}{\lambda(nm) \times I_{inc}\left(\frac{\mathrm{W}}{\mathrm{cm^2}}\right)} \times 100$$

The electrochemical impedance spectroscopy (EIS) was performed on a CH 660C electrochemical analyzer (CH Instruments, Shanghai, China) in a two electrode configuration. The photoanode was used as a working electrode and the Pt electrode as a counter electrode. The electron transport properties were investigated using electrochemical impedance spectroscopy (EIS) with 10 mV alternative signal in the frequency range of 10^{-2} – 10^{5} Hz. Electron transport time and electron lifetimes were measured by intensity-modulated photocurrent spectroscopy (IMPS) and intensity-modulated photovoltage spectroscopy (IMVS) with same electrochemical workstation (CH 660C electrochemical analyzer). The electrochemical workstation is equipped with a red LED source (635 nm) which is used as light source for the above studies. Photovoltage response of the cells were studied in the frequency range of 1 Hz to 1 kHz. The cell was illuminated with sinusoidal modulated light containing 10% of the DC component. IMPS and IMVS were measured at different bias light intensities.

Preparation of TiO_2 electrode (photoanode) and counter electrode

A TiO_2 film electrode (photoanode) was prepared by TiO_2 highly transparent paste (Titanium-HT) provided by Solaronix spreading on conducting glass plate (15Ω/cm^2, Pillkington, USA) by doctor's blade method and annealed at 450°C for half an hour in air. The dyes were adsorbed to the TiO_2 surface by immersing the TiO_2 coated electrodes in dichloromethane solution of dyes for 12 h. The un-adsorbed dyes were washed up with dichloromethane. Platinum counter electrode was prepared by deposition of Pt catalyst T/SP paste (purchased from Solaronix SA) on another conducting glass and annealed at 400°C for half an hour in air.

DSSC assembly

In DSSCs assembly the platinum catalyst-coated counter electrode was placed on the top so that the conductive side of the counter electrode faces the dye coated TiO_2 film and the cell was sealed by three sides by using spacer SX1170-60,50µm (solaronix) and leave the one side open for the injection of electrolyte solution. The iodide electrolyte solution (0.1M Lithium iodide mixed with 0.01M iodine in acetonitrile) was placed at the edges of the plates. The liquid was drawn into the space between the electrodes by capillary action. Using araldite the remaining open part of the cell assembly was sealed and made the contact by copper wire by using silver paste and then sealed the contact by araldite.

Syntheses

(*E*)-3-ferrocenylacrylic acid (D1)

Compound (*E*)-3-ferrocenylacrylic acid (**D1**) was prepared in accordance with the previously reported procedure.[44] Ferrocene carboxyaldehyde (0.512 g, 2 mmol) and malonic acid (0.311 g, 2.99 mmol) were added and dissolved in 2 mL of freshly distilled pyridine followed by addition of 1-2 drops of piperidine. The resulting solution was refluxed at 108 °C with stirring for 6 hours under nitrogen atmosphere during which the evolution of CO_2 stopped. The obtained reaction mixture was cooled slowly to room temperature followed by washing with 2N HCl and thereafter extracted with 5% NaOH 3-4 time. The sodium hydroxide extracts were combined and was acidified with 6N HCl. A brick-red precipitate was formed upon complete acidification, which was collected by filtration and washed with distilled water thoroughly to remove traces of acid and finally the residue was dried under vacuum.

Yield: 0.354g, 69.14% (red solid). m. p. 193°C. ^{1}H NMR (DMSO-d6, 300MHz): δ 12.05 (s, 1H, COOH), 7.42 (d, 1H), 6.07 (d, 1H), 4.66 (2H, FcCH2), 4.44 (2H, FcCH2), 3.86 (s, 5H, Fc); ^{13}C NMR (DMSO-*d6*, 75.50 MHz): δ 168.0 (-COOH), 145.0 (C-COOH), 116.0 (C=C), 79.0 (Fc-CH), 71.0 (4C, Fc), 69.8 (5C, Fc). FT-IR (KBr, cm^{-1}): ν 3070 (C-H), 1668 (COOH), 1610 (C=C), 487 (Fe-Cp ring); Calcd. For $C_{13}H_{12}O_2Fe$ (%): C 60.97, H 4.72. Found C 61.02, H 4.82.

Synthesis of (*E*)-2-(4-hydroxyphenyl)-5-(2-ferrocenyl-ethen-1-yl)-1,3,4-oxadiazole **(D2)**

D1 (0.064 g, 0.25 mmol) and triethylamine (0.175g, 0.25 mmol) were dissolved in dichloromethane (3.5 mL) and the resulting solution was stirred for 10 minutes followed by addition of dichloromethane suspension of 4-hydroxybenzhydrazide (0.038 g, 0.25 mmol) and TBTU (1.1 equiv, 0.26 mmol) under nitrogen

atmosphere. The resulting mixture was stirred 20 h at room temperature. Thereafter triethylamine (0.051, 0.5 mmol) was added, followed by addition of 4-methylbenzenesulfonyl chloride (0.143 g, 0.75 mmol). The obtained reaction mixture was stirred for another 12 hour and after that the reaction was quenched by adding 14% aqueous ammonia solution. The stirring was continued for an additional 45 minutes. The product was extracted with dichloromethane: water. To remove traces of 4-methylbenzenesulfonamide, the organic layer was treated with a 2N NaOH solution. The obtained organic layer was washed with water and kept in anhydrous sodium sulfate for 4 h, filtered and vacuum evaporated to dryness and finally the product was washed with diethyl ether.

Yield: 0.170 g, 47.3 % (dark red solid), m. p. 220°C (d). ^{1}H NMR ($CDCl_3$, 300 MHz) δ: 8.08 (d, 1H), 7.97 (d, 1H), 7.64 ((d, 2H, C_6H_5), 7.42 (d, 2H, C_6H_4), 4.65 (2H, Fc), 4.33 (2H, Fc), 4.15 (s, 5H, Fc). ^{13}C NMR ($CDCl_3$, 75.50 MHz) δ: 150.4 (C-OH, C_6H_5), 148.1 (C=N-N=C), 139.1 (C-O-), 129.17 (-C=C-), 128.3 (CH-C_6H_4), 69.0 (Fc-C), 68.8 (Fc-4C), 67.1 (Fc, 5C). FTIR (KBr, cm^{-1}): ν 3490 (OH-C_6H_4), 2962 (C-H), 1604 (C=C), 1490 (C=N-N=C, oxadiazole), 1261, (C-O-C, oxadiazole), 486 (Fe-Cp). Calcd. For $C_{20}H_{16}O_2N_2Fe$ (372.0561) (%): C 64.54, H 4.33, N 7.53. Found C 65.02, H 4.76, N 8.12. HRMS (ESI): *m/z* = 373.0620 $[M+H]^+$.

Synthesis of (*E*)-2-(4-nitrophenyl)-5-(2-ferrocenyl-ethen-1-yl)-1,3,4-oxadiazole (**D3**)

A similar procedure was adopted to synthesize **D3** except that instead of 4-hydroxybenzhydrazide, 4-nitrobenzhydrazide (0.046 g, 0.25 mmol) was taken.

Yield: 0.199 g, 50% (dark red solid), m. p. 212 °C (d). ^{1}H NMR ($CDCl_3$, 300 MHz) δ: 8.36 (d, 1H), 8.22 (d, 1H), 7.51 (d, 2H, C_6H_4), 7.45 (d, 2H, C_6H_4), 4.52 (2H, Fc), 4.42 (2H, Fc), 4.16 (5H, Fc). ^{13}C NMR ($CDCl_3$, 7.50 MHz) δ: 165.5 (C-NO_2), 163.8 (C=N-N=C), 149.8 (C-O), 129.5, 128.5, 127.6 (C=C, C_6H_4), 71.7 (C-CH, Fc), 70.0 (2C, Fc), 69.1 (2C, Fc), 68.3 (5C, Fc). FTIR (KBr, cm^{-1}) ν: 2962 (C-H), 1631 (C=C), 1519 (asymm NO_2), 1431 (C=N-N=C, oxadiazole), 1338 (symm NO_2), 1259 (C-O-C, oxadiazole), 482 (Fe-Cp). Calcd. For $C_{20}H_{15}FeN_3O_3$ (401.0463) (%): C 59.87, H 3.77, N 10.47. Found C 60.73, H 4.01, N 10.84. HRMS (ESI): *m/z* = 402.0520 $[M+H]^+$.

Synthesis of (*Z*)-N'-hydroxyimidamide

4-Nitrobenzonitrile (0.297 g, 2 mmol) and hydroxylamine hydrochloride (0.129 g, 4 mmol) were dissolved in ethanol (5 mL). The resulting solution was stirred under nitrogen and $NaHCO_3$ (0.336 g, 4 mmol) dissolved in 4.6 mL water was added dropwise to the stirring solution. The obtained yellow coloured solution was stirred at room temperature for 24 h and the reaction was monitored using TLC. Thereafter the solvent vacuum evaporated. The compound was extracted with ethyl acetate and water. The obtained fluorescent yellow solution was kept in anhydrous sodium sulfate and filtered, the solvent was removed by rotary evaporation and product was vacuum dried.

Yield: 0.325 g, 98.0% m. p. 180˚C. ^{1}H NMR (DMSO-d_6, 300 MHz, δ): 10.15 (s, 1H, N-OH), 8.24 (dd, 2H, C_6H_4), 7.95 (dd, 2H, C_6H_4), 6.08 (br, 2H, NH_2); ^{13}C NMR (DMSO-d_6, 75.50 MHz, δ): 166.7 (C=N-OH), 150.4 (C-NH2), 140.4 (C-NO_2, C6H4), 137.3 (2C, C_6H_4), 129.3 (2C, C_6H_4), 123.9 (C-NH_2).

Synthesis of Ethyl 3-aryl-1,2,4-oxadiazole-5-carboxylate

N,N'-diisopropylethylamine (0.480 g, 3.6 mmol) was added dropwise to the stirring THF solution of amidoxime (0.303 g, 1.8 mmol) in an ice bath (5 °C) under nitrogen. Ethyl oxalyl chloride (2.16 ml, 1.8 mmol) was added to the mixture and this was stirred for 10 minutes. The temperature of the reaction mixture was brought upto room temperature and then the reaction mixture was refluxed for 150 min under nitrogen atmosphere. After completion of reaction, the reaction mixture was cooled on ice-bath and 2N HCl (1.8 mL) was added dropwise to it. Thereafter, the product was extracted with ethyl acetate (4×25 mL) and water (100 mL). The obtained dark yellow organic layer was washed with aqueous sodium bicarbonate and dried over anhydrous sodium sulfate. The solvent was removed under reduced pressure and the crude product was purified using column chromatography (silica 60-120), using hexane:ethyl acetate (88:12, V/V).

Yield: 0.892 g, 97%, m.p. 120˚C. 1H NMR ($CDCl_3$, 300 MHz, δ): 8.30 (dd, 2H, C_6H_4-NO_2), 7.76 (dd, 2H, C_6H_4), 4.56 (q, 2H, CH_2), (1.58, t, 3H, CH_3); ^{13}C NMR ($CDCl_3$, 75.50 MHz, δ): 166.8 (COO), 152.7 (C=N, oxadiazole), 148.8 (C-NO_2), 132.4 (-C- oxadiazole), 127.7 (2C, C_6H_4), 123.2 (2C, C_6H_4), 63.2 (CH_2), 13.0 (CH_3).

Synthesis of aryl oxadiazole-5-carbohydazide

Hydrazine monohydrate (0.212 g, 4.24 mmol) was added in the ethanol solution (5.3 ml) of ethyl aryl carboxylate (0.558 g, 2.12 mmol). A cream-yellow precipitate of hydrazide was readily formed. The mixture was stirred for 2 h at room temperature. The obtained precipitate was filtered and washed with cold ethanol.

Yield: 0.558 g, 99%, m.p. 197˚C (d). ^{1}H NMR (DMSO-d_6, 300 MHz, δ): 10.95 (s, N-H), 8.45 (d, 2H, C_6H_4), 8.31 (d, 2H, C_6H_4), 4.97 (br, 2H, NH_2); ^{13}C NMR (DMSO-d_6, 75.50 MHz, δ): 180.2 (CONH), 170.0 (C-O-N=C), 167.1 (C=N-), 151.8 (C-NO_2) , 131.8 (C-oxadiazole), 129.0 (2C, C_6H_4), 125.0 (2C, C_6H_4).

Synthesis of (*E*)-3-(4-nitrophenyl)-5-[5-(2-ferroceneylethen-1-yl)-1,3,4-oxadiazol-2-yl]-1,2,4-oxadiazole (D4)

A similar procedure was adopted to synthesize **D4** as used for the syntheses of **D2** and **D3** except that instead of 4-hydroxybenzhydrazide, aryl oxadiazole-5-carbohydazide (0.046 g, 0.25 mmol) was taken.

Yield: 0.118 g, 50% (Red solid) m.p. 280˚C (d).^{1}HNMR ($CDCl_3$, 300MHz):δ 8.36 (d, 1H), 8.28 (d, 1H), 7.73 (2H, d, C_6H_4), 6.68 (2H, C_6H_4), 4.55 (2H, Fc), 4.48 (2H, Fc), 4.15 (s, 5H, Fc).^{13}CNMR ($CDCl_3$, 75.50 MHz): δ 127.6 (C=C, C_6H_4), 123.1 (C=C, C_6H_4), 70.5 (CH-Fc), 68.7 (2C, Fc), 67.4 (2C, Fc), 64.7 (5C, Fc).FT-IR (KBr, cm^{-1}): ν 2962 (C-H), 1641 (C=C), 1523

(aymmNO$_2$), 1450 (C=N-N=C, oxadiazole), 1350 (symmNO$_2$), 1261 (C-O-C, oxadiazole), 489 (Fe-Cp). Calcd. For $C_{22}H_{15}FeN_5O_4$ (469.0473) (%): C 56.31, H 3.22, N 14.93. Found C 57.03, H 3.45, N 15.01. HRMS (ESI): *m/z* = 470.0529 $[M+H]^+$.

X-ray Crystallography

Intensity data for **D1** were collected at 150(2) K on a Rigaku Xcalibur, EosS2 single crystal diffractometer using graphite monochromated Mo-Kα radiation (λ = 0.71073 Å). For **D4** on a Rigaku Supernova Dual, EosS2 system using monochromated Cu-Kα radiation (λ = 1.54184 Å). Unit cell determination, data collection and data reduction were performed using the CrysAlisPro software.[45] An empirical absorption correction using spherical harmonics was employed. The structures were solved with SHELXT[46] and refined by a full-matrix least-squares procedure based on F^2 (SHELXL-2018/3).[46] All non-hydrogen atoms were refined anisotropically. Hydrogen atoms were placed onto calculated positions and refined using a riding model.

Crystal Data **D1**. $C_{13}H_{12}FeO_2$, M = 256.08, Monoclinic, $P2_1/n$, a = 8.6991(3) Å, b = 11.5638(4) Å, c = 11.4461(4) Å, β = 110.945(4)° V = 1075.34(7) Å^3, Z = 4, D_{calc} = 1.582 mg m^{-3}, F(000) = 528, crystal size 0.600 × 0.400 × 0.200 mm, reflections collected 9009, independent reflections 2797 [$R_{(int)}$ = 0.0258], Final indices [I> 2σ(I)] R_1 = 0.0349, wR_2 = 0.0770, R indices (all data) R_1 = 0.0408, wR_2 = 0.0806, gof 1.036, Largest difference peak and hole 0.884 and -0.266 e Å^{-3}. **CCDC No. 1882088**.

Crystal Data **D4**. $C_{22}H_{15}FeN_5O_4$, M = 469.24, Monoclinic, $P2_1/n$, a = 5.9928(3) Å, b = 8.5610(5) Å, c = 37.157(3) Å, β = 91.337(5)° V = 1905.80(19) Å^3, Z = 4, D_{calc} = 1.635 mg m^{-3}, F(000) = 960, crystal size 0.12 × 0.05 × 0.04 mm, reflections collected 19880, independent reflections 19880 [$R_{(int)}$ = ?], Final indices [I> 2σ(I)] R_1 = 0.0939, wR_2 = 0.2041, R indices (all data) R_1 = 0.1297, wR_2 = 0.2280, gof 1.104, Largest difference peak and hole 0.734 and -0.484 e Å^{-3}. **CCDC No. 1882089**.

Note: the entire molecule is disordered over two sites in the ratio 1:1. Due to the proximity of the two parts which overlap in most cases ADP restraints had to be applied for all atoms and geometric constraints for the C-ring atoms. The crystal did not diffract well to high angles which lead to weak high angle data which explains the high R-value. Additionally, the structure was refined as a 2-component twin 180.0° rotation about 6. 0. -1 reciprocal lattice direction.

Computational details

In order to ascertain the nature of electronic transition in the ferrocenyl oxadiazole, compounds density functional theory (DFT) calculations were performed. Optimized molecular geometries were calculated using the B3LYP exchange-correlation functional.[47, 48] The MDF10 basis set for Fe and 6-31G** basis set for other atoms were used for geometry optimization. All the calculations were performed using Gaussian 09 programme.[49] The TiO_2 cluster$(TiO_2)_{30}$+**D1-D4** system was optimized by using 3-21G* basis set and initial geometry were taken from the relaxed geometry of $(TiO_2)_{30}$ cluster and **D1-D4**.

Conflicts of interest

There are no conflicts to declare.

Acknowledgements

RC is grateful to Department of Science and Technology for the INSPIRE fellowship IFA-12CH-34. AK is grateful to Council of Scientific and Industrial Research, New Delhi for the financial assistance in the form of project no. 01(2899)/17/EMR-II.

Notes and references

‡ Footnotes relating to the main text should appear here. These might include comments relevant to but not central to the matter under discussion, limited experimental and spectral data, and crystallographic data.

1 B. O'Regan, M. Grätzel, *Nature*, 1991, **353**, 737–740.

2 (a) A. Hagfeldt, G. Boschloo, L. C. Sun, L. Kloo and H. Pettersson, *Chem. Rev*., 2010, **110**, 6595–6663; (b) B. Bozic-Weber, E. C. Constable and C. E. Housecroft, *Coord. Chem. Rev.*, 2013, **257**, 3089; (c) M. K. Nazeeruddin, A. Kay, I. Rodicio, R. Humphry-Baker, E. Meller, P. Liska, N. Vlachopoulos and M. Grätzel, *J. Am. Chem. Soc.*, 1993, **115**, 6382; (d) M. K. Nazeeruddin, S. M. Zakeeruddin, R. Humphry-Baker, M. Jirousek, P. Liska, N. Vlachopoulos, V. Ahklover, C. H. Fischer and M. Grätzel, *Inorg. Chem.*, 1999, **38**, 6298; (e) M. K. Nazeeruddin, F. D. Angelis, S. Fantacci, A. Selloni, G. Viscardi, P. Liska, S. Ito, B. Takeru and M. Grätzel, *J. Am. Chem. Soc.*, 2005, **127**, 16835; (f) M. Grätzel, *J. Photochem. Photobiol. A*, 2004, **164**, 3; (g) M. K. Nazeeruddin, P. Pechy, T. Renouard, S. M. Zakeeruddin, R. Humphry-Baker, P. Comte, P. Liska, L. Cevey, E. Costa, V. Shklover, L. Spiccia, G. B. Deacon, C. A. Bignozzi and M. Grätzel, *J. Am. Chem. Soc.*, 2001, **123**, 1613; (h) G. Boschloo and A. Hagfeldt, *Acc. Chem. Res*., 2009, **42**, 1819-1826.

3 L. Y. Han, A. Islam, H. Chen, C. Malapaka, B. Chiranjeevi, S. F. Zhang, X. D. Yang and M. Yanagida, *Energy Environ. Sci*. 2012, **5**, 6057−6060.

4 K. Kakiage, Y. Aoyama, T. Yano, K. Oya, J. Fujisawa and M. Hanaya, *Chem. Commun*. 2015, **51**, 15894−15897.

5 B. O'Regan, K. Walley, M. Juozapavicius, A. Anderson, F. Matar, T. Ghaddar, S. M. Zakeeruddin, C. Klein and J. R. Durrant, *J. Am. Chem. Soc.*, 2009, **131**, 3541–3548.

6 F. Gao, Y. Wang, D. Shi, J. Zhang, M. Wang, X. Jing, R. Humphry-Baker, P. Wang, S. M. Zakeeruddin and M. Grätzel, *J. Am. Chem. Soc.*, 2008, **130**, 10720–10728.

7 D. Kuang, S. Ito, B. Wenger, C. Klein, J. E. Moser, R. Humphry-Baker, S. M. Zakeeruddin and M. Grätzel, *J. Am. Chem. Soc.*, 2006, **128**, 4146–4154.

8 (*a*) C. Y. Chen, M. Wang, J. Y. Li, N. Pootrakulchote, L. Alibabaei, C. H. Ngoc-le, J. D.Decoppet, J. H. Tsai, C. Gratzel, C. G. Wu, S. M. Zakeeruddin and M. Gratzel, *ACS Nano*, 2009, **3**, 3103−3109; (*b*) S. Aghazada, P. Gao, A. Yella, G. Marotta, T. Moehl, J. Teuscher, J. E. Moser, F. De Angelis, M. Gratzel and M. K. Nazeeruddin, *Inorg. Chem.* 2016, **55**, 6653−6659; (c) Y. Huang, W-C. Chen, X-X. Zhang, R. Ghadari, X-Q. Fang, T. Yu and F-T. Kong, *J. Mater. Chem. C*, 2018, **6**, 9445-9452.

9 (*a*) H. Choi, S. Paek, N. Lim, Y. H. Lee, M. K. Nazeeruddin, J. Ko , *Chem. Eur. J.* 2014, **20**, 10894−10899; (*b*)T. Meng, C. Liu, K. Wang, T. He, Y. Zhu, A. A. Enizi, A. Elzatahry and X. Gong, *ACS Appl. Mater. Interfaces*, 2016, **8**, 1876−1883; (c) H. Yin, S. Chen, S. H. Cheung, H. W. Li, Y. Xie, S. W. Tsang, X. Zhu and S. K. Ko, *J. Mater. Chem. C*, 2018, **6**, 9111-9118; (d) A. Magomedov, E. Kasparavičius, K. Rakstys, S. Paek, N. Gasilova, K. Genevičius, G. Juška, T. Malinauskas, M. K. Nazeeruddin and V. Getautis, *J. Mater. Chem. C*, 2018, **6**, 8874-8878; (e) S. Sidhik, A. C. Pasarán, C. R. Pérez, T. López-Luke and E. D. la Rosa, *J. Mater. Chem. C*, 2018, **6**, 7880-7889.

10 (*a*) M. Liang and J. Chen, *Chem. Soc. Rev*. 2013, **42**, 3453−3488;(*b*) Z. Yang, C. Shao and D. Cao, *RSC Adv*. 2015, **5**, 22892−22898;(*c*) S. H. Chou, C. H. Tsai, C. C. Wu, D. Kumar and K. T. Wong, *Chem. Eur. J.* 2014, **20**, 16574−16582; *(d)* Y. Ooyama and Y. Harima, *Eur. J. Org. Chem*. 2009, **2009**, 2903−2934.

11 A. Kumar, R. Chauhan, K. C. Molloy, G. Kociok-Köhn, L. Bahadur and N. Singh, *Chem. Eur. J.*, 2010, **16**, 4307.

12 V. Singh, R. Chauhan, A. N. Gupta, V. Kumar, M. G. B. Drew, L. Bahadur and N. Singh, *Dalton Trans.*, 2014, **43**, 4752–4761.

13 R. Yadav, M. Trivedi, G. Kociok-Köhn, R. Chauhan, A. Kumar and S. W. Gosavi, *Eur. J. Inorg. Chem.*, 2016, 1013–1021.

14 (a) R. Chauhan, M. Trivedi, R. Yadav, A. Kumar, D. P. Amalnerkar, S. W. Gosavi, *Spectrochim. Acta A: Mol. Biomol. Spectro.*, 2015, **150**, 652–656; (b) R. Yadav, Y. Waghadkar, G. Kociok-Köhn, A. Kumar, S. B. Rane and R. Chauhan, *Optical Materials*, 2016, **62**, 176-183.

15 V. Singh, R. Chauhan, A. Kumar, L. Bahadur and N. Singh, *Dalton Trans.*, 2010, **39**, 9779–9788.

16 R. Chauhan, G. Kociok-Köhn, M. Trivedi, S. Singh, A. Kumar and D. P. Amalanerkar, *J. Solid State Electrochem.*, 2015, **19**, 739–747.

17 R. Chauhan, S. Auvinen, A. S. Aditya, M. Trivedi, R. Prasad, M. Alatalo, D. P. Amalnerkar and A. Kumar, *Sol. Energy*, 2014, **108**, 560–569.

18 R. Chauhan, M. Trivedi, L. Bahadur and A. Kumar, *Chem.-Asian J.*, 2011, **6**, 1525–1532.

19 R. Chauhan, M. Shahid, M. Trivedi, D. P. Amalnerkar and A. Kumar, *Eur. J. Inorg. Chem.*, 2015, 3700–3707.

20 R. Chauhan, R. Yadav, A. K. Singh, M. Trivedi, G. Kociok-Köhn, A. Kumar, S. Gosavi and S. Rane, *RSC Adv.*, 2016, **6**, 97664-97675

21 R. Yadav, A. Singh, G. Kociok-Köhn, R. Chauhan, A. Kumar and S. Gosavi, *New J. Chem.*, 2017, **41**, 7312-7321.

22 A. Singh, P. Singh, G. Kociok-Köhn, M. Trivedi, A. Kumar, R. Chauhan, S. B. Rane, C. Terashima, S. W. Gosavi and A. Fujishima, *New J. Chem.*, 2018, **42**, 9306-9316.

23 (a) R. Misra, R. Maragani, K. R. Patel and G. D. Sharma, *RSC Adv.*, 2014, **4**, 34904–34911; (b) R. Maragani, R. Misra, M. S. Roy, M. K. Singh, G. D. Sharma, *Phy. Chem. Chem. Phy.*, 2017, **19**, 8925-8933.

24 D. Sirbu, C. Turta, A. C. Benniston, F. Abou-Chahine, H. Lemmetyinen, N. V. Tkachenko, C. Wood and E. Gibson, *RSC Adv.*, 2014, **4**, 22733–22742.

25 M. Cariello, S. Ahn, K.-W. Park, S.-K. Chang, J. Hong and G. Cooke, *RSC Adv.*, 2016, **6**, 9132–9138.

26 Ferrocenes: Ligands, Materials and Biomolecules, ed. P. Stepnicka, John Wiley and Sons Ltd., 2008.

27 A. Hildebrandt, T. Ruffer, E. Erasmus, J. C. Swarts and H. Lang, *Organometallics*, 2010, **29**, 4900–4905.

28 V. N. Nemykin, G. T. Rohde, C. D. Barrett, R. G. Hadt, C. Bizzarri, P. Galloni, B. Floris, I. Nowik, R. H. Herber, A. G. Marrani, R. Zanoni and N. M. Loim, *J. Am. Chem. Soc.*, 2009, **131**, 14969–14978.

29 A. Auger and J. C. Swarts, *Organometallics*, 2007, **26**, 102–109.

30 J. Conradie, T. S. Cameron, M. A. S. Aquino, G. J. Lamprecht and J. C. Swarts, *Inorg. Chim. Acta*, 2005, **358**, 2530–2542.

31 A. Auger, A. J. Muller and J. C. Swarts, *Dalton Trans.*, 2007, 3623–3633.

32 (a) A. Paun, N. D. Hadade, C. C. Paraschivescu and M. Matache, *J. Mater. Chem. C*, 2016, **4**, 8596-8610; (b) R. M. Ongunal, A. P. Sivadas, N. S. S. Kumar, S. Menon and S. Das, *J. Mater. Chem. C*, 2016, **4**, 8596-8610.

33 K. Srinivas, G. Sivakumar, Ch. R. Kumar, M. A. Reddy, K. Bhanuprakash, V. J. Rao, C-W. Chen, Y-C. Hsu and J. T. Lin, *Synth. Met.*, 2011, **161**, 1671-1681.

34 H. Wang, H. Liu, F.-Q. Bai, S. Qu, X. Jia, X. Ran, F. Chen, B. Bai, C. Zhao, Z. Liu, H.-X. Zhang and M. Li, *J. Photochem. Photobiol. A*, 2015, **312**, 20.

35 (a) J. C. P. Meyer, A. C. Sauer, B. A. Iglesias, T. V. Acunha, D. F. Back, O. E. D. Rodrigues and L. Dornelles, *J. Organomet. Chem.*, 2017, **841**, 1-11; (b) G. T. Cin, G. Verep, S. D. Topel and V. Ciger, *Chem. Heterocyclic Comp.*, 2013, **49**, 1138-1144; (c) A. R. Kazemizadeh, N. Shajari, R. Shapouri, N. Adibpour, R. T.-Mofrad, P. Dinmo-Hammadi, *Appl. Organometal. Chem.*, 2016, **30**, 148-153.

36 Y. S. Sohn, D. N. Hendrickson and H. B. Gray, *J. Am. Chem. Soc.*, 1971, **93**, 3603–3612.

37 G. Janssens, F. Touhari, J. W. Gerritsen, H. V. Kempen, P. Callant, G. Deroover and D. Vandenbroucke, *Chem. Phys. Lett.*, 2001, **344**, 1–6.

38 C. Y. Lin, C. F. Lo, L. Luo, H. P. Lu, C. S. Hung and E. W. G. Diau, *J. Phys. Chem.*, 2009, **113**, 755–764.

39 K. E. Naveen, R. Jose, P. S. Archana, C. Vijila, M. M. Yusoff and S. Ramakrishna, *Energy Environ. Sci.*, 2012, 5, 5401–5407.

40 K. E. Naveen, R. Jose, P. S. Archana, C. Vijila, M. M. Yusoff and S. Ramakrishna, *Energy Environ. Sci.*, 2012, **5**, 5401–5407.

41 S. Ashoka, G. Nagaraju, C. N. Tharamani and G. T. Chandrapp, *Mater. Lett.*, 2009, **63**, 873–876.

42 J. Lin, Y. U. Heo, A. Nattestad, Z. Sun, L. Wang, J. H. Kim and S. X. Dou, *Sci. Rep.*, 2014, **4**, 5769.

43 Q. Wang, J. E. Moser and M. Grätzel, *J. Phys. Chem. B*, 2005, **109**, 14945–14953

44 N. H. Nemeroff, M.E. McDonnell, J. M. Axten and L. J. Buckley, *Synt. Commun.*, 1992, **22**, 3271-3275.

45 CrysAlisPro 1.171.39.46 (Rigaku Oxford Diffraction, 2018).

46 G. M. Sheldrick, *Acta Cryst*., 2015, **C71**, 3–8.

47 A. D. Becke, *J. Chem. Phys.*, 1993, **98**, 5648.

48 C. T. Lee, W. T. Yang and R. G. Parr, *Phys. Rev. B: Condens. Matter Mater. Phys.*, 1998, **37**, 1133.

49 M. J. Frisch, G. W. Trucks, H. B. Schlegel, G. E. Scuseria, M. A. Robb, J. R. Cheeseman, J. A. Montgomery, T. Vreven Jr., K. N. Kudin, J. C. Burant, J. M. Millam, S. S. Iyengar, J. Tomasi, V. Barone, B. Mennucci, M. Cossi, G. Scalmani, N. Rega, G. A. Petersson, H. Nakatsuji, M. Hada, M. Ehara, K. Toyota, R. Fukuda, J. Hasegawa, M. Ishida, T. Nakajima, Y. Honda, O. Kitao, H. Nakai, M. Klene, X. Li, J. E. Knox, H. P. Hratchian, J. B. Cross, V. Bakken, C. Adamo, J. Jaramillo, R. Gomperts, R. E. Stratmann, O. Yazyev, A. J. Austin, R. Cammi, C. Pomelli, J. W. Ochterski, P. Y. Ayala, K. Morokuma, G. A. Voth, P. Salvador, J. J. Dannenberg, V. G. Zakrzewski, S.

Dapprich, A. D. Daniels, M. C. Strain, O. Farkas, D. K. Malick, A. D. Rabuck, K. Raghavachari, J. B. Foresman, J. V. Ortiz, Q. Cui, A. G. Baboul, S. Clifford, J. Cioslowski, B. B. Stefanov, G. Liu, A. Liashenko, P. Piskorz, I. Komaromi, R. L. Martin, D. J. Fox, T. Keith, M. A. Al-Laham, C. Y. Peng, A. Nanayakkara, M. Challacombe, P. M. W. Gill, B. Johnson, W. Chen, W. M. Wong, C. Gonzalez, J. A. Pople, Gaussian 09 (Gaussian, Inc., Wallingford CT, revision B.01 2009).